Grain-scale stress heterogeneity in concrete from in-situ X-ray measurements

Mohmad M. Thakur[a], N. Axel Henningsson[b], Jonas Engqvist[b], Pierre-Olivier Autran[c], Jonathan P. Wright[c], Ryan C. Hurley[a,d,e,]

[a]*Hopkins Extreme Materials Institute, Johns Hopkins University, Baltimore, MD 21218, USA*
[b]*Division of Solid Mechanics, Lund University, Box 118, 221 00 Lund, Sweden*
[c]*ESRF-The European Synchrotron, 71 Avenue des Martyrs, 38000 Grenoble, France*
[d]*Department of Mechanical Engineering, Johns Hopkins University, Baltimore, MD 21218, USA*
[e]*Department of Civil and Systems Engineering, Johns Hopkins University, Baltimore, MD 21218, USA*

Abstract

Concrete features significant microstructural heterogeneity which affects its mechanical behavior. Strain localization in the matrix phase of concrete has received significant attention due to its relation to microcracking and our ability to quantify it with X-ray computed tomography (XRCT). In contrast, stresses in sand and aggregates remain largely unmeasured but remain critical for micromechanics-based theories of failure. Here, we use a combination of *in-situ* XRCT, 3D X-ray diffraction (3DXRD), and scanning 3DXRD to directly measure strain and stress within sand grains in two samples of mortar containing different sand volume fractions. Our results reveal that, in contrast to inclusion theories from continuum micromechanics, aggregates feature a broad distribution of average stresses and significant gradients in their internal stress fields. Our work furnishes the first known dataset with these quantitative stress measurements and motivates improvements in micromechanics models for concrete which can capture stress heterogeneity.

Keywords: Concrete, Aggregate Stresses, Scanning 3D X-ray Diffraction, 3D X-ray Diffraction, Heterogeneity,

1. Introduction

Concrete is a heterogeneous material consisting of aggregates and a matrix of cement paste. Prior work has revealed significant heterogeneity in the microstructure and material properties of the cement paste [1, 2]. Experimental techniques such as nanoindentation provide an estimate of elastic properties of different phases in concrete [3]. These measurements provide input material properties for mesoscale models which are used to predict the mechanical response of concrete from its microstructure [4]. Recent studies coupled these mesoscale models and experiments

Email addresses: mthakur3@jh.edu (Mohmad M. Thakur), rhurley6@jhu.edu (Ryan C. Hurley)

with *in-situ* imaging to provide microscale data for validating mesoscale models, [5] marking the first effort to validate mesoscale models directly at the microscale, rather than relying on comparisons with macroscale measurements. However, most mesoscale models continue to be validated based only on a comparison of their predicted macroscopic stress-strain response with experimental measurements or with an additional measurement of microscale damage localization profile in the cement paste [6, 7]. In all but only a few prior studies [8, 9], the evolution of stresses in aggregates during macroscopic loading remained unmeasured. The reliability of mesoscale and continuum micromechanics models, which depend on assumptions regarding the aggregate stress distributions to predict failure (e.g., [10, 11]), therefore remains to be validated.

The use of mesoscale modeling or experiments with *in-situ* imaging remains confined to small samples, typically not larger than 20 mm in any dimension. Continuum micromechanics on the other hand has emerged as a promising tool for predicting the mechanical response of large volumes of material while accounting for microstructural heterogeneity. Konigsberger and colleagues [12, 10] developed a multiscale micromechanics model to determine the traction at the aggregate surfaces to infer 3D stress states in the surrounding interfacial transition zones (ITZ). They further predicted the location of the largest tensile stresses in the ITZ surrounding aggregates by assuming them to be spherical and their stresses to be derivable from Eshelby's inclusion theory. This location and the corresponding tensile stresses were assumed to drive fracture nucleation and thus concrete strength. A central assumption in their approach and in many other micromechanics-inspired continuum models is that the stress inside each aggregate and average stress in all the aggregates follows from Eshelby's inclusion theory – intra-aggregate stresses are gradient free and all aggregates in a material feature the same stress derivable from Eshelby's theory [13, 14].

In this work, we address the following questions that are essential to developing robust mesoscale and continuum micro-mechanics models for concrete: (1) Are the stresses in different aggregates in a sample of concrete the same? If not, how significant is the variation in stresses and does it depend on the aggregate volume fraction? (2) How significantly do stresses vary inside each aggregate in a sample of concrete? Answering this question is critical for understanding stress and strain localization in ITZ. (3) What fraction of the aggregates exhibit stresses greater than the mean stress? One previous work [9] clarified that continuum micromechanics models provide accurate estimates of global aggregate average stress for concrete samples with low aggregate volume fraction (≈ 0.15) but did not examine the stress variations inside individual aggregates.

To answer these questions, we performed unconfined compression experiments on two samples composed of ordinary portland cement mixed with water and quartz sand with varying volume fractions. We refer to these samples as concrete, although the term "micro-concrete" has also been used in the literature to refer to specimens containing such small aggregate sizes [15]. We used *in-situ* x-ray computed tomography imaging (XRCT), 3D x-ray diffraction

(3DXRD), and scanning 3D x-ray diffraction (s3DXRD) measurements to capture the microstructure of concrete, determine the average stress in each aggregate, and determine stress variation within aggregates, respectively. To the best of our knowledge, these experiments represent the first dataset resolving stress variations within aggregates in a concrete sample. This communication is arranged as follows. Section 2 describes the experiments. Section 3 discusses results. Section 4 provides a conclusion.

2. Experiments and In-situ X-ray Imaging

Two concrete samples, referred to as S1 and S2, with aggregates consisting of single-crystal quartz grains, were prepared using Ordinary Portland Cement (OPC) and ball- and air-milled single crystal quartz with aggregate volume fractions equal to 20% and 30%. A water-to-cement ratio of approximately 0.5 by weight was used for each sample. A detailed description of the experiments and sample preparation, including the preparation of single-crystal quartz grains, is described in [5]. Here, we only review salient information for the current study. We note that the single-crystal quartz grains are chemically and morphologically similar to siliceous sands typically used to make cement; however, the former is ideal for X-ray diffraction measurements because it provides well-defined diffraction spots for analysis.

Unconfined uniaxial compression experiments were performed at the ID11 beamline of the European Synchrotron Radiation Facility (ESRF) [5]. Stress-strain curves are shown in Figure 1. We performed a combination of XRCT imaging and 3DXRD measurements at the consecutive compressive load states marked in Figure 1 (a). We performed s3DXRD measurements only for sample S1 at compressive loads equal to 83 N ($\sigma_{zz} \approx 26$ MPa) and 99.5 N ($\sigma_{zz} \approx 32$ MPa). Although, sample S2 exhibited yielding as evident by the softening in Figure 1 (a), we restrict our discussion to load cases before yielding. Prior work discussed XRCT imaging and 3DXRD measurements in detail [16]. XRCT provided the microstructure of the samples at a resolution of 2.5 microns/voxel. 3DXRD measurements provided a single stress tensor for each aggregate (single-crystal quartz grain) in the concrete sample. Here we revisit this data and also discuss s3DXRD, used to determine intra-grain stress fields in each aggregate [17], to address the questions posed in the Section 1.

s3DXRD is a variant of 3DXRD which employs a square X-ray beam smaller than the size of individual crystals to probe samples [18, 17]. By virtue of the small beam size, the sequential sample rotation and lateral translation of samples, and reconstruction methods exploiting tomographic principles, we can measure intra-granular crystal orientations, and strain fields with s3DXRD with approximately 10^{-4} resolution per strain tensor component. Stress fields can readily be determined from these strain fields using the anisotropic form of Hooke's law (the crystal orientation can be computed from the diffraction measurement).

s3DXRD measurements were made using a 20×20 μm box beam. A total of 180 diffraction images were acquired during a 180° rotation of the sample such that each frame was integrated continuously over a 1-degree interval. After each 180° rotation, the sample was translated horizontally 20 μm in a direction orthogonal to the X-ray beam path to illuminate a distinct portion of the sample, and another 180° rotation was performed. We continued this sequence of scans and translations 35 times to scan a 700 μm diameter and 20 μm tall section of the center of the sample. We then translated the sample 20 μm upward and repeated the process. A total of 20 non-overlapping layers were scanned in this manner so that a 400 μm tall portion of the sample was examined. This 400 μm portion of the sample began at the approximate center of the sample's height and extended downward in the laboratory reference frame (positive z in Figure 1). The s3DXRD data was refined in ImageD11, using methods described in [17] and methods similar to those described in [19], to obtain orientation, strain, and stress on a voxel-by-voxel basis at a resolution of 20 μm throughout the 400 μm tall portion of the sample which was scanned.

3. Results and Discussion

The data from XRCT, 3DXRD, and s3DXRD were registered to assign an average stress tensor from 3DXRD and an intra-granular stress field from s3DXRD to each aggregate observed in the XRCT images. Registration was performed by translating and rotating grain centroids (and respective tensor quantities such as stress) obtained from each method, as described in [16], until they were within 30 μm of one another. Grains in the XRCT dataset without a registered 3DXRD grain were assigned a stress tensor equal to the mean of registered grains. Grains in the XRCT dataset without a registered s3DXRD grain were not considered for analysis of intra-granular stresses. Figures S1 and S2 in the supplementary data demonstrate close alignment of XRCT and 3DXRD grain positions and XRCT and s3DXRD grain positions, respectively.

3.1. Stresses from 3D X-ray Diffraction (3DXRD)

Figure 1 (a) shows the macroscopic stress-strain response of Sample S1 and S2. Sample S2 had a higher aggregate volume fraction compared to sample S1 and therefore exhibited a stiffer response. There was also a slight variation in the water-to-cement ratio of the two samples, as discussed in prior work [5].

Figures 1 (b) - (g) show the average σ_{zz}^{agg} for all grains measured using 3DXRD and successfully registered to XRCT grains at several load levels. An aggregate's stress tensor was computed from its strain tensor and grains were assumed strain-free at the first load step of the experiment (reference loads of 7 N and 0 N for samples S1 and S2, respectively). Although not exact, this strain-free assumption eliminates errors due to slight variations in strain-free lattice constants of the quartz grains. It can be observed from Figure 1 that the average aggregate stresses increased

with the macroscopic load. Furthermore, average aggregate stresses for different aggregates were heterogeneous and not uniform as assumed in continuum micromechanics models.

The heterogeneity of average aggregate stresses increased with macroscopic loads, as reflected by a broadening of the σ_{zz}^{agg} distributions in Figure 2. The standard deviation of σ_{zz}^{agg} for Sample S1 was 17 MPa, 24 MPa, and 30 MPa at macroscopic loads of 43 N (σ_{zz}= 24 MPa) , 63 N (σ_{zz}= 36 MPa), and 83 N (σ_{zz}= 47 MPa), respectively. The standard deviation of σ_{zz}^{agg} for Sample S2 was equal to 32 MPa, 41 MPa, and 58 MPa at macroscopic loads of 50 N (σ_{zz}= 28 MPa), 70 N (σ_{zz}= 40 MPa), and 90 N (σ_{zz}= 51 MPa), respectively. Sample S2, which had a higher aggregate volume fraction, in particular, exhibited a higher standard deviation. The distribution of other stress components for Sample S1 and S2 are provided in Figures S3 and S4, respectively, in the supplementary data. We observed that the fraction of grains with σ_{zz}^{agg} stresses more negative (compressive) than the mean aggregate stress was approximately 40% for both samples at all load steps, as shown in Figure S5 in the supplementary data. In a granular material, such grains would be called force chains. To the best of our knowledge, such force chains have not yet been measured or modeled in concrete, but concepts of force chains in granular materials have enabled new continuum micromechanics models with enhanced predictive capabilities [20].

3.2. Stresses from Scanning 3D X-ray Diffraction (s3DXRD)

s3DXRD measurements were reconstructed at 20 μm resolution on a voxel-by-voxel basis in a 400 μm tall section of Sample S1, as described in Section 2. Figure 3 (a) provides a rendering of the 51 grains for which s3DXRD measurements were successfully made. Approximately 20 grains were registered with XRCT data; the remainder were not registered most likely because of our stringent criterion for matching XRCT and s3DXRD grains combined described in Section 2 combined with the fairly coarse (20 μm) spatial resolution of s3DXRD data, and because the region interrogated with s3DXRD was smaller than the full sample diameter and thus the reconstruction of grains overlapping the boundary of this region would feature inaccurate centers. s3DXRD grains were segmented by binarizing the voxelized data and applying a watershed segmentation algorithm [16]. Figures 3 (b) and (c) show the intra-aggregate σ_{zz} stress components on the 20 μm grid for each grain at two load levels. These figures qualitatively convey significant intra-granular heterogeneity of σ_{zz} which is further supported quantitatively by the frequency distribution of intra-aggregate σ_{zz} stress for a select number of grains at both macroscopic loads in Figure 3 (d). We note that the stress distributions within individual aggregates is heterogeneous and *not* uniform as would be assumed in a continuum micromechanics model employing an infinite-domain Eshelby inclusion theory [21, 9]. The maximum and minimum standard deviation of σ_{zz} within individual aggregates was 24 MPa and 8 MPa for a macroscopic load equal to 83 N, and 30 MPa and 10 MPa for a macroscopic load equal to 99.5 N.

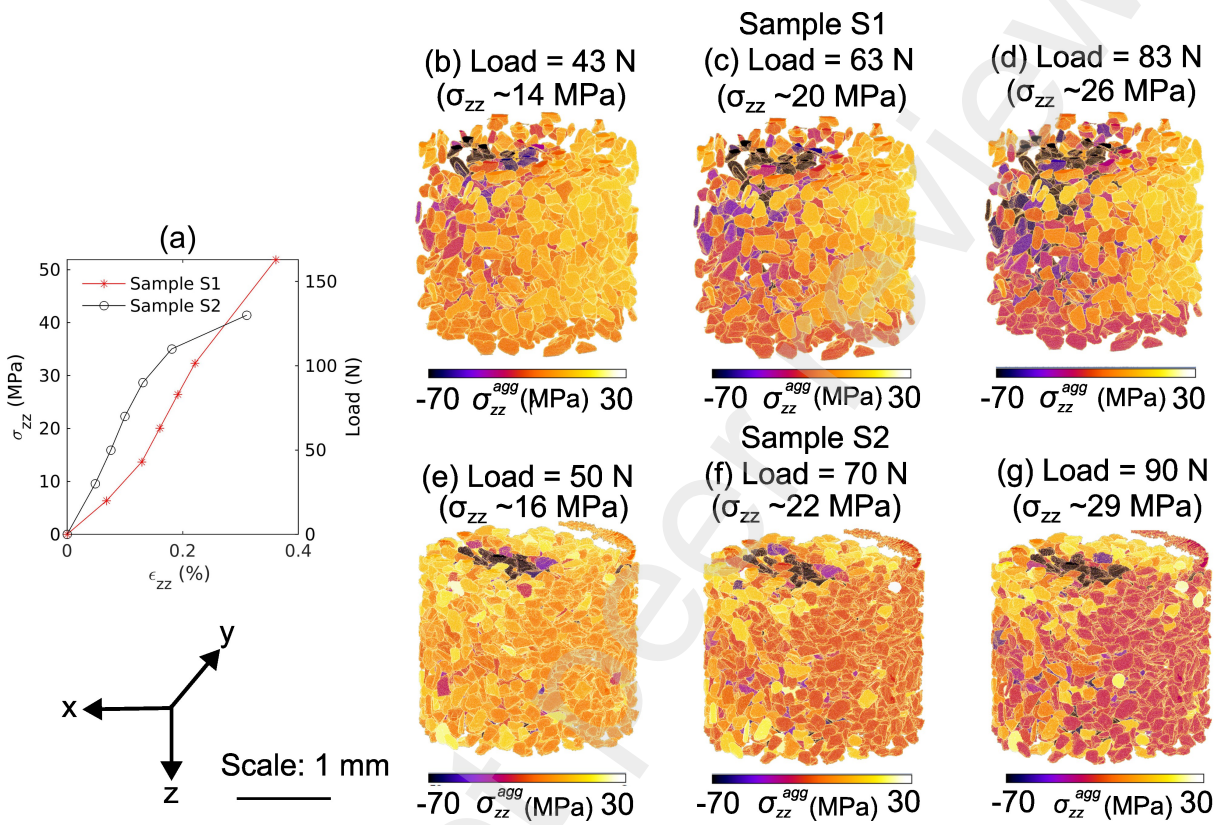

Figure 1: (a) Average aggregate stresses and load cell reading at several sample strains for Samples S1 and S2. At each symbol, the sample strain was held constant while XRCT and 3DXRD measurements were made. At symbols correponding to 83 N and 99.5 N for Sample S1, we performed s3DXRD measurements in addition to XRCT and 3DXRD measurements. Average individual aggregate stresses in both samples are shown in (b) - (g). (b) Sample S1 with macroscopic load = 43 N. (c) Sample S1 with macroscopic load = 63 N. (d) Sample S1 with macroscopic load = 83 N. (e) Sample S2 with macroscopic load = 50 N. (f) Sample S2 with macroscopic load = 70 N. (g) Sample S2 with macroscopic load = 90 N.

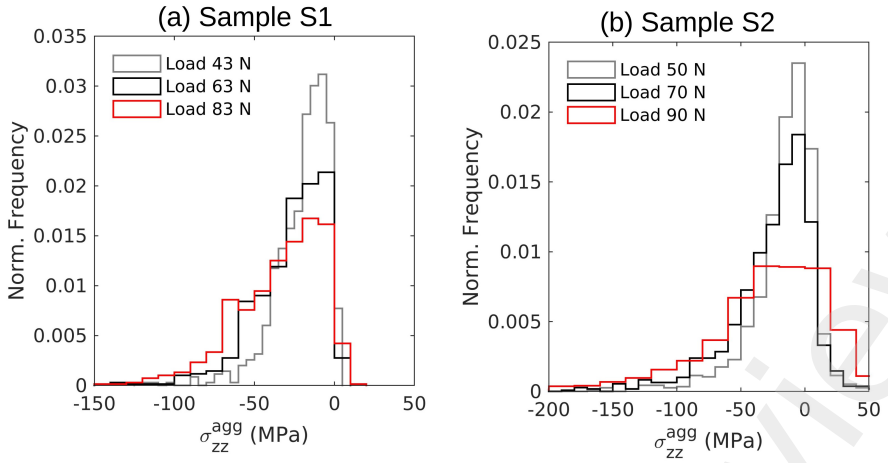

Figure 2: Histograms of average individual aggregate stresses (σ_{zz}) for different macroscopic loads obtained from 3D X-ray Diffraction. (a) Sample S1 . (b) Sample S2.

Heterogeneity in intra-aggregate stresses, in contrast to expectations from micromechanics theories, may stem from multiple sources: (1) deviation from an ellipsoidal inclusion shape for the aggregates, which invalidates the Eshelby assumption; (2) finite domains, which modify Eshelby's tensor and introduce intra-aggregate stress gradients [22]; (3) strong aggregate-mortar or aggregate-aggregate interaction effects, which are incorporated implicitly into Mori-Tanaka's theory but not into Eshelby's inclusion theory [22]. To assess whether deviation from ellipsoidal shapes alone plays a role in causing stress gradients, we plot the standard deviation of intra-granular stress versus a measure of deviation from ellipsoidal shape in Figure 3 (d). The ellipticity parameter, (Es) defined in [23], was obtained from XRCT images for grains that were registered with scanning 3DXRD. The deviation of Es from 1 indicates deviation in ellipticity of a grain. We find no clear trend, and no significant reduction of standard deviation at Es=1, suggesting that the shape alone does not cause significant intra-granular stress gradients. The finite domain size would not alone cause the observed intra-granular stress gradient because each grain features a distinct stress distribution. We therefore conclude that some combination of shape, finite-domain, and interaction effects likely contribute to the intra-granular stress gradients. We conclude that care must be taken when applying continuum micromechanics models assuming constant intra-aggregate stresses to the prediction of concrete mechanics and failure [21, 10, 24, 9].

4. Conclusion

Few direct measurements of aggregate stresses and no intra-aggregate stress measurements have been made until now [8, 9]. These quantities are employed in micromechanics models for predicting elastic properties and incipient

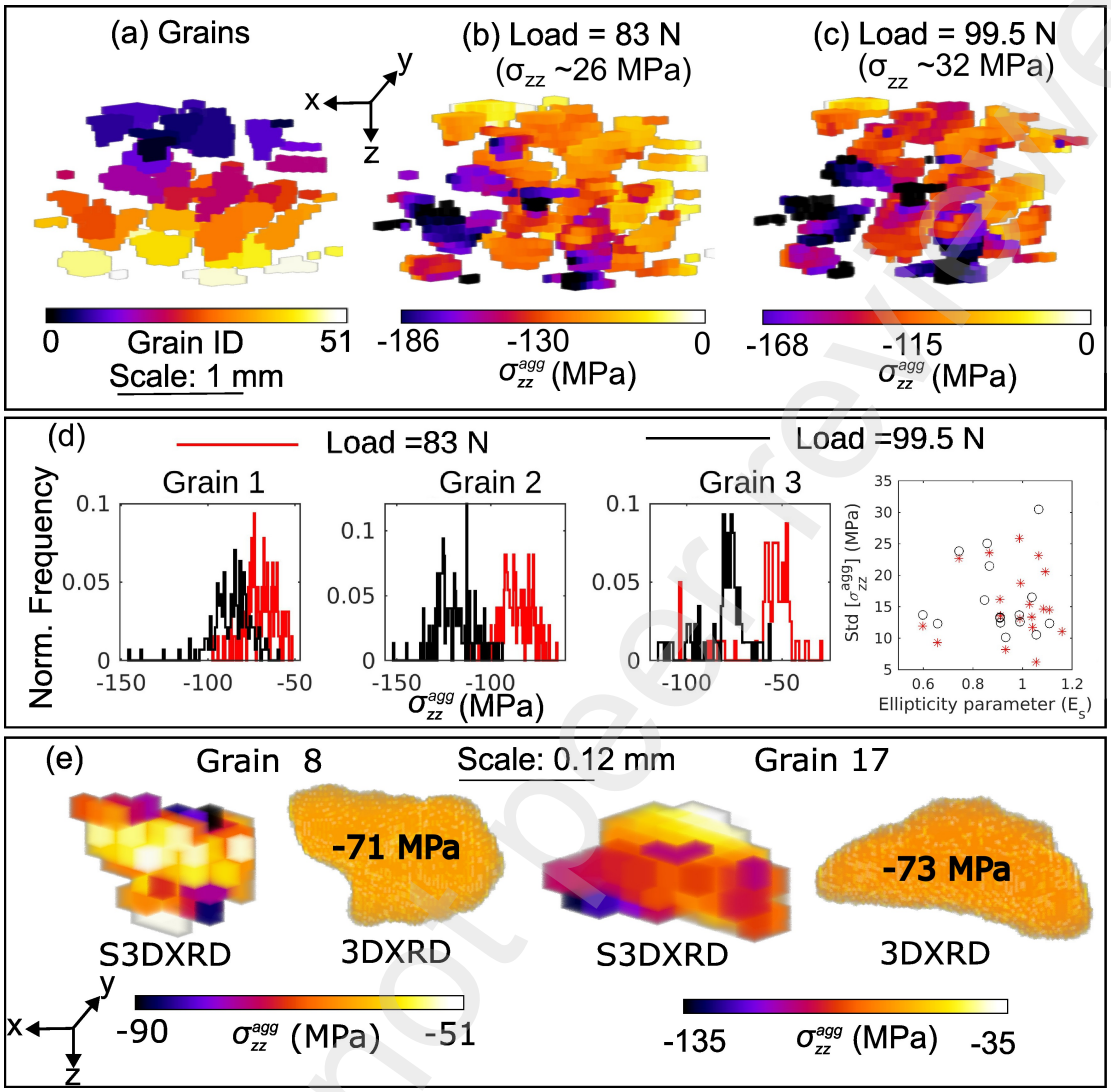

Figure 3: Stresses (σ_{zz}) inside aggregates obtained from scanning 3D X-ray Diffraction (s3DXRD). (a)Individual aggregates obtained from (s3DXRD). (b)Visualization of σ_{zz} field for macroscopic load = 83 N. (c) Visualization of σ_{zz} field for macroscopic load = 99.5 N. (d) Distribution of σ_{zz}in some individual aggregates for macroscopic load = 83 N and 99.5 N and standard deviation of stresses (σ_{zz}) inside aggregates with the variation in shape (ellipticity) of aggregates. (e) Close visualization of σ_{zz}field for macroscopic load = 83 N obtained from s3DXRD and 3DXRD

failure and can also be employed to calibrate mesoscale models [21, 10, 24, 5]. Here, we employed XRCT, 3DXRD, and s3DXRD to furnish microstructure, average stresses, and intra-granular stresses for the first time in a small specimen of concrete. Key findings are as follows:

1. The average stresses in aggregates measured with 3DXRD exhibited significant heterogeneity, in contrast with predictions of Eshelby's inclusion theory for infinite domains. Approximately 40 % of the aggregates exhibited compressive stresses more negative than the mean, reflecting force chain like behavior akin to that of granular media.

2. Intra-aggregate σ_{zz} fields exhibited significant gradients in contrast to Eshelby's inclusion theory for infinite domains. Grain morphology, finite domain sizes, and aggregate-mortar or aggregate-aggregate interaction effects may have each contributed to the presence of these gradients.

3. Regardless of origin, intra-aggregate stress gradients suggest a need for micromechanics models to incorporate heterogeneity for robust predictions.

Acknowledgements

MMT and RCH acknowledge support by the U.S. National Science Foundation Award No. CMMI-2125023. All authors acknowledge support from ESRF for synchrotron beamtime under proposal numbers ma-4978.

Competing Interests

The authors declare no competing interests.

Data availability

Data used for this work is provided at www.zenodo.org [25].

References

[1] S. Diamond, The microstructure of cement paste and concrete - A visual primer, Cement and Concrete Composites 26 (8) (2004) 919–933. doi:10.1016/j.cemconcomp.2004.02.028.

[2] V. S milauer, Z. Bittnar, Microstructure-based micromechanical prediction of elastic properties in hydrating cement paste, Cement and Concrete Research 36 (9) (2006) 1708–1718. doi:10.1016/j.cemconres.2006.05.014.

[3] K. Velez, S. Maximilien, D. Damidot, G. Fantozzi, F. Sorrentino, Determination by nanoindentation of elastic modulus and hardness of pure constituents of Portland cement clinker, Cement and Concrete Research 31 (4) (2001) 555–561. doi:10.1016/S0008-8846(00)00505-6.

[4] M. A. Homel, J. Iyer, S. J. Semnani, E. B. Herbold, Cement and Concrete Research Mesoscale model and X-ray computed micro-tomographic imaging of damage progression in ultra-high-performance concrete, Cement and Concrete Research 157 (October 2021) (2022) 106799. doi:10.1016/j.cemconres.2022.106799.
URL https://doi.org/10.1016/j.cemconres.2022.106799

[5] M. M. Thakur, N. A. Henningsson, J. Engqvist, P.-O. Autran, J. P. Wright, R. C. Hurley, On mesoscale modeling of concrete: Role of heterogeneities on local stresses, strains, and representative volume element, Cement and Concrete Research 163 (2023) 107031.

[6] Y.-j. Huang, S. Natarajan, H. Zhang, F.-q. Guo, S.-l. Xu, C. Zeng, Z.-s. Zheng, A ct image-driven computational framework for investigating complex 3d fracture in mesoscale concrete, Cement and Concrete Composites 143 (2023) 105270.

[7] S. Naderi, W. Tu, M. Zhang, Meso-scale modelling of compressive fracture in concrete with irregularly shaped aggregates, Cement and concrete research 140 (2021) 106317.

[8] R. Hurley, D. Pagan, An in-situ study of stress evolution and fracture growth during compression of concrete, International Journal of Solids and Structures 168 (2019) 26–40.

[9] R. C. Hurley, D. C. Pagan, E. B. Herbold, C. Zhai, Examining the micromechanics of cementitious composites using in-situ x-ray measurements, International Journal of Solids and Structures 267 (2023) 112162.

[10] M. Königsberger, B. Pichler, C. Hellmich, Micromechanics of itz-aggregate interaction in concrete part ii: Strength upscaling, Journal of the American Ceramic Society 97 (2) (2014) 543–551.

[11] M. Königsberger, M. Hlobil, B. Delsaute, S. Staquet, C. Hellmich, B. Pichler, Hydrate failure in itz governs concrete strength: A micro-to-macro validated engineering mechanics model, Cement and Concrete Research 103 (2018) 77–94.

[12] M. Königsberger, B. Pichler, C. Hellmich, Micromechanics of ITZ-aggregate interaction in concrete part I: Stress concentration, Journal of the American Ceramic Society 97 (2) (2014) 535–542. doi:10.1111/jace.12591.

[13] K. Tanaka, Note on volume integrals of the elastic field around an ellipsoidal inclusion, J. elasticity 2 (1972) 199–200.

[14] J. D. Eshelby, The determination of the elastic field of an ellipsoidal inclusion, and related problems, Proceedings of the royal society of London. Series A. Mathematical and physical sciences 241 (1226) (1957) 376–396.

[15] O. Stamati, E. Roubin, E. Andò, Y. Malecot, P. Charrier, Fracturing process of micro-concrete under uniaxial and triaxial compression: Insights from in-situ X-ray mechanical tests, Cement and Concrete Research 149 (June) (2021) 106578. doi:10.1016/j.cemconres.2021.106578.

[16] M. M. Thakur, S. Enright, R. C. Hurley, Phase segmentation in x-ray ct images of concrete with implications for mesoscale modeling, Construction and Building Materials 403 (2023) 133033.

[17] N. A. Henningsson, S. A. Hall, J. P. Wright, J. Hektor, Reconstructing intragranular strain fields in polycrystalline materials from scanning 3dxrd data, Applied Crystallography 53 (2) (2020) 314–325.

[18] Y. Hayashi, D. Setoyama, Y. Seno, Scanning three-dimensional x-ray diffraction microscopy with a high-energy microbeam at spring-8, in: Materials Science Forum, Vol. 905, Trans Tech Publ, 2017, pp. 157–164.

[19] A. Henningsson, M. Kutsal, J. P. Wright, W. Ludwig, H. O. Sørensen, S. A. Hall, G. Winther, H. F. Poulsen, Microstructure and stress mapping in 3d at industrially relevant degrees of plastic deformation, Scientific Reports 14 (1) (2024) 20213.

[20] A. Gupta, K. Ramesh, R. Hurley, An inclusion model for predicting granular elasticity incorporating force chain mechanics, Granular Matter 26 (2) (2024) 40.

[21] M. Königsberger, B. Pichler, C. Hellmich, Micromechanics of ITZ-Aggregate Interaction in Concrete Part II: Strength Upscaling 97 (2) (2014) 543–551. doi:10.1111/jace.12606.

[22] S. Li, G. Wang, Introduction to micromechanics and nanomechanics by Shaofan Li, Gang Wang (z-lib.org) (2008).

[23] Y. Hayakawa, T. Oguchi, Evaluation of gravel sphericity and roundness based on surface-area measurement with a laser scanner, Computers

& geosciences 31 (6) (2005) 735–741.

[24] M. Königsberger, M. Hlobil, B. Delsaute, S. Staquet, C. Hellmich, B. Pichler, Hydrate failure in ITZ governs concrete strength: A micro-to-macro validated engineering mechanics model, Cement and Concrete Research 103 (November 2017) (2018) 77–94. doi:10.1016/j.cemconres.2017.10.002.
URL https://doi.org/10.1016/j.cemconres.2017.10.002

[25] M. M. Thakur, N. A. Henningsson, J. Engqvist, P.-O. Autran, J. P. Wright, R. C. Hurley, Dataset for article titled "grain-scale stress heterogeneity in concrete from in-situ x-ray measurements", Zenodo, https://doi.org/10.5281/zenodo.14003326, deposited: 2024-10-29 (2024).

Supplemental Material: Grain-scale stress heterogeneity in concrete from in-situ X-ray measurements

This supplementary materials document contains additional figures to support the results and discussion of the communication associated with this document.

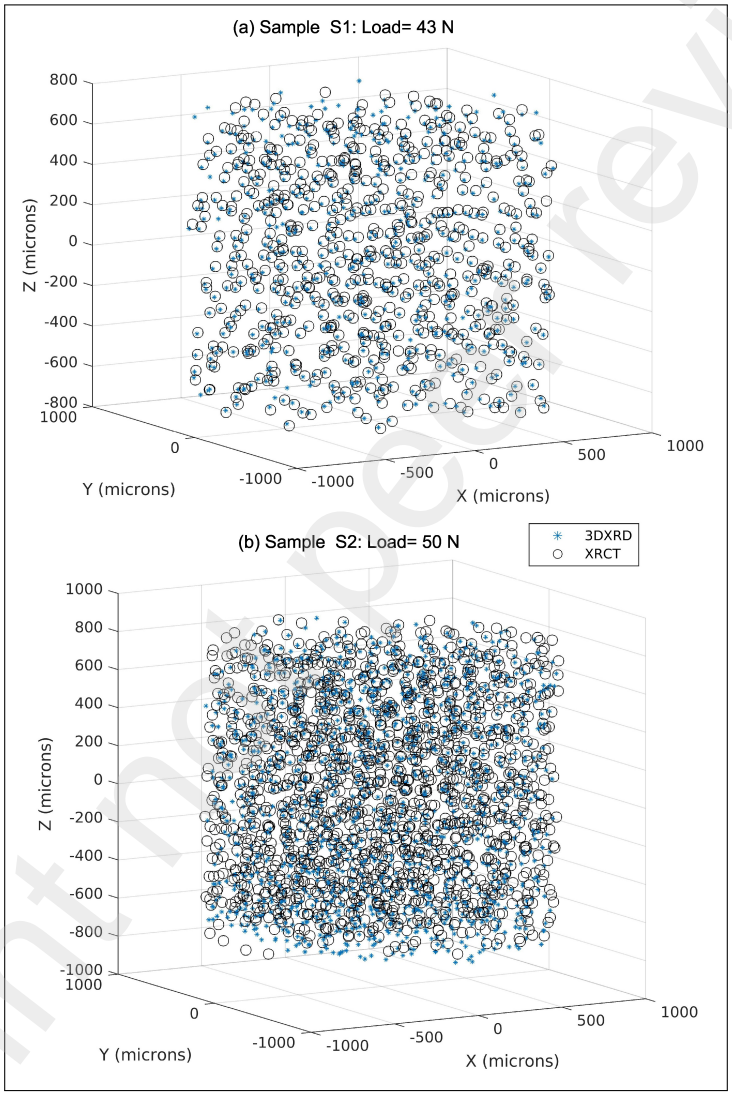

Fig. S1. Centroids of grains showing registration of x-ray computed tomography imaging (XRCT) and 3D x-ray diffraction (3DXRD). (a) Sample S1. (b) Sample S2.

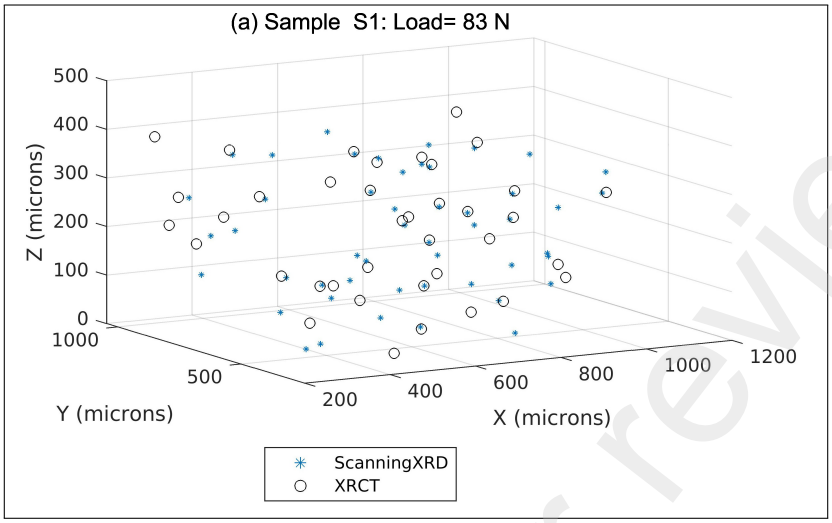

Fig. S2. Centroids of grains showing registration of x-ray computed tomography imaging (XRCT) and scanning 3DXRD (s3DXRD) for Sample S1.

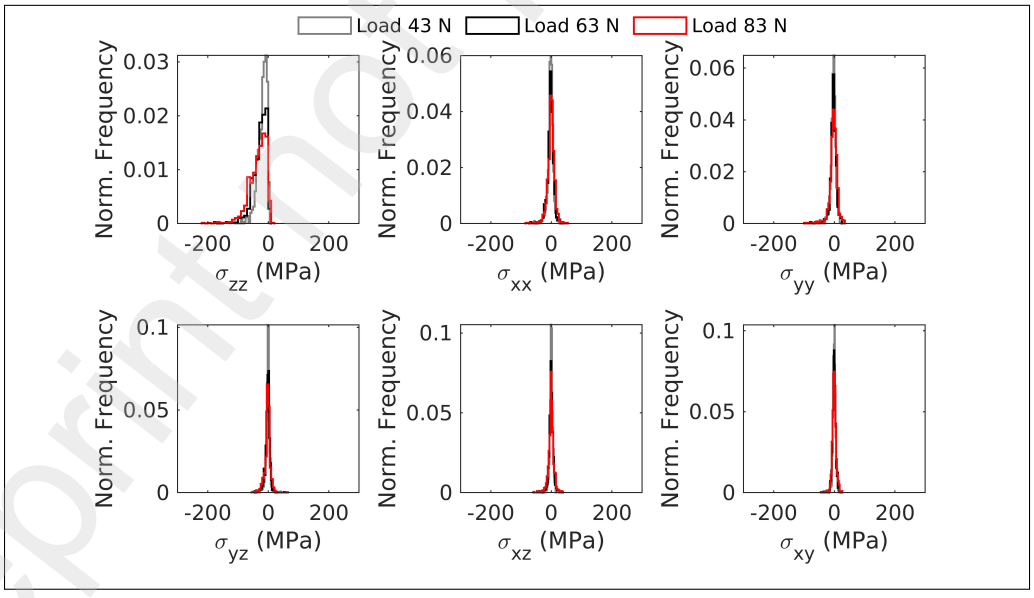

Fig. S3. Distribution of components of average individual aggregate stresses for different macroscopic loads obtained from 3DXRD for sample S1.

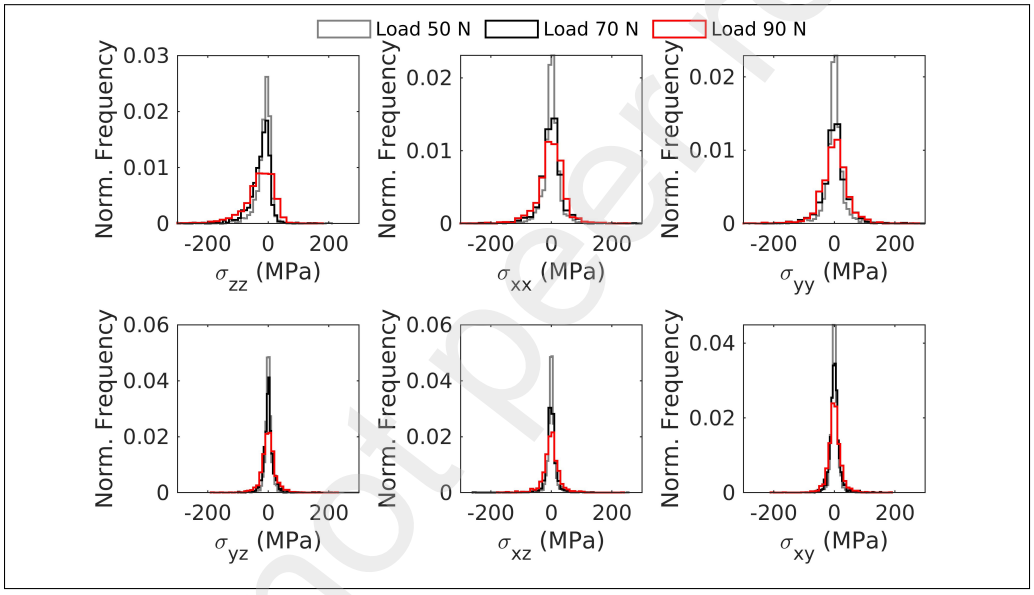

Fig. S4. Distribution of components of average individual aggregate stresses for different macroscopic loads obtained from 3DXRD for sample S2.

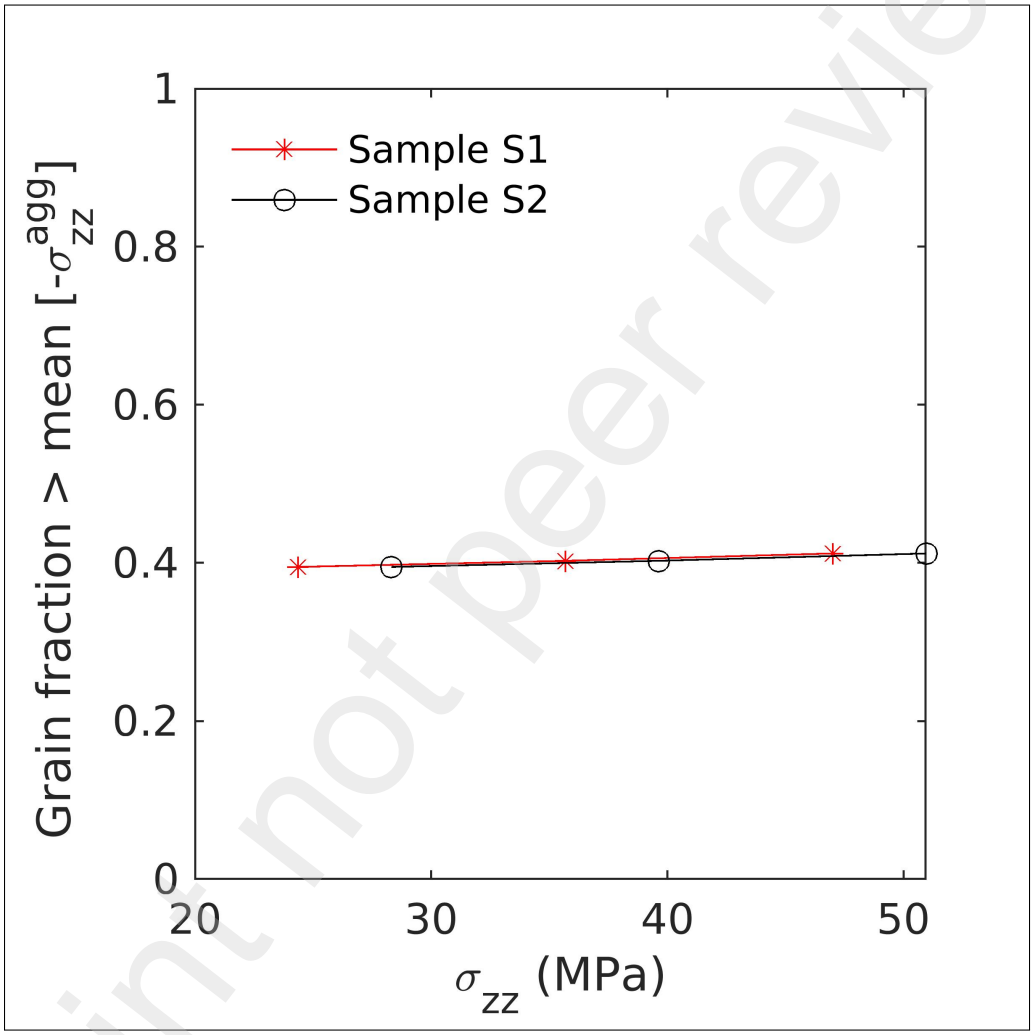

Fig. S5. Fraction of grains with σ_{zz}^{agg} stresses more negative (compressive) than the mean aggregate stress for Samples S1 & S2 at different levels of macroscopic average stress (x-axis.

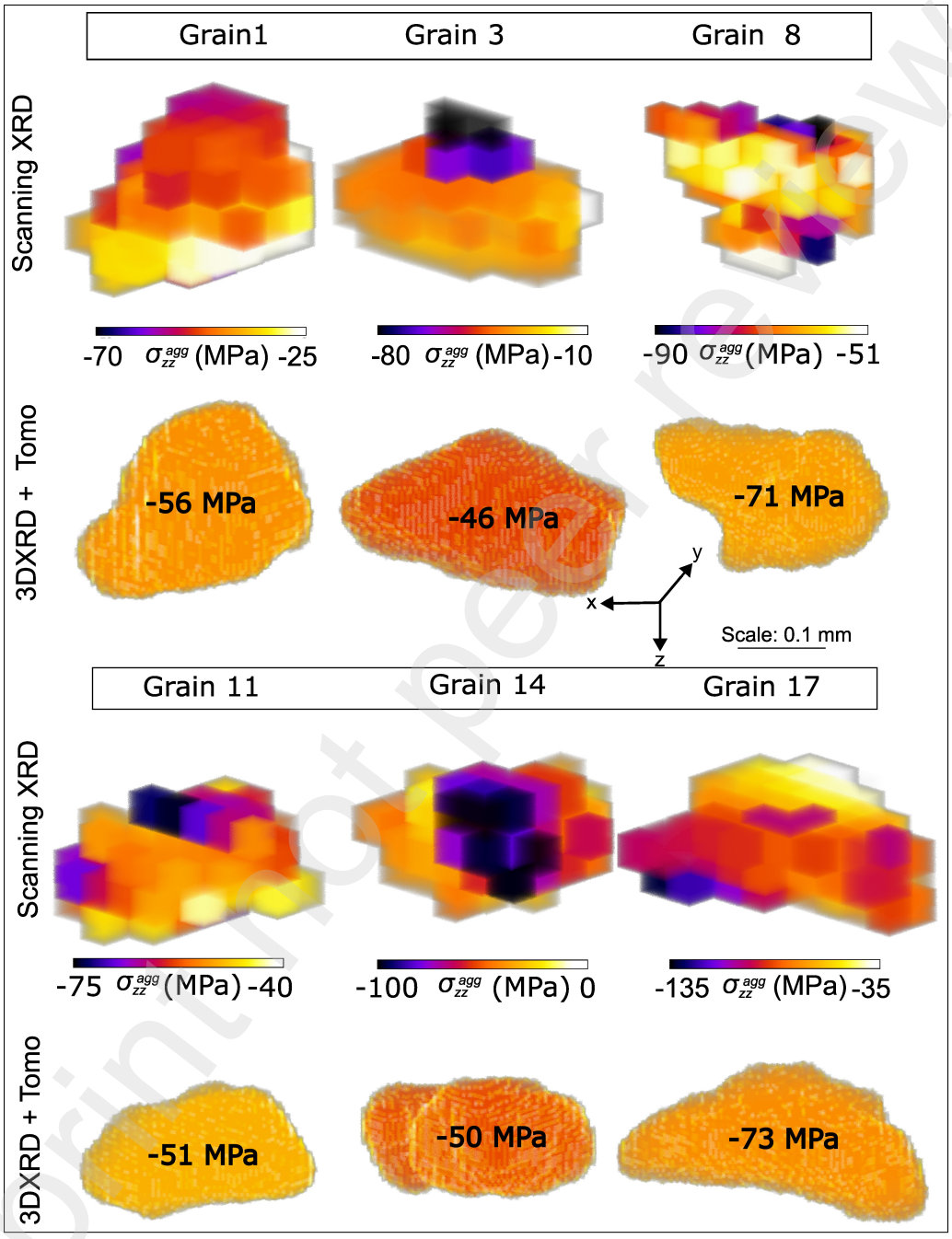

Fig. S6. Close visualization of intra-aggregate σ_{zz} field for macroscopic load of 83 N obtained from s3DXRD for Sample S1. For comparison, the grain stress obtained for the corresponding grain from 3DXRD is plotted below each s3DXRD rendering.